Geomechanics for Energy and the Environment xxx (xxxx) xxx

Contents lists available at ScienceDirect

Geomechanics for Energy and the Environment

journal homepage: www.elsevier.com/locate/gete

Experimental characterization and numerical modeling of the self-weight consolidation of a dredged mud

Bertrand François *, Gilles Corda

Université Libre de Bruxelles, BATir Department, Brussels, Belgium

ARTICLE INFO

Article history:
Received 18 March 2021
Received in revised form 12 August 2021
Accepted 9 September 2021
Available online xxxx

Editors-in-Chief:
Professor Lyesse Laloui and Professor Tomasz Hueckel

Keywords:
Large strain consolidation
Dredged mud
Experimental characterization
Permeability
Compressibility
Finite difference method

ABSTRACT

The kinetics of one-dimensional self-weight consolidation of dredged mud depends on the permeability and the compressibility of the mud, in addition to the height of the mud and the drainage conditions at the boundaries. The process is highly non-linear because of the drastic variation of permeability and compressibility during the densification of the mud. In this work, we investigate the self-weight consolidation of a mixed sediments, dredged from the Belgian rivers and channels and discharged in disposal site

First of all, this study proposes two original experiments, the hydraulic column and the kinematic permeameter, to determine the two constitutive relations governing this self-weight consolidation. A power law is used to relate the permeability with the void ratio of the mud, while a hyperbolic function is preferred for the relation between void ratio and vertical effective stress. Additionally, self-weight consolidation tests of dredged mud are performed in plexiglass column, drained at the base through a layer of sand. The settlement of the mud–water interface and the excess pore water pressure profile are monitored during the tests.

In addition to this experimental characterization, the Gibson's large strain consolidation equation is solved through a finite difference method to evaluate the ability of the constitutive relations to reproduce the kinetics of self-weight consolidation observed in the consolidation column. Finally, sensitivity analysis of the constitutive relations of the mud is carried out. The model reproduces quite well the evolution of the excess pore water pressure profile in the mud, while the rate of settlement of the mud–water interface is overestimated by the model at very short term. Also, it is observed that the draining sand at the base plays an insignificant role on the speed of consolidation if the permeability of this sand remains lower that the permeability of the mud at the densified state.

1. Introduction

Freight transport by inland navigation is of paramount importance for many industrial activities in the world. The number and the size of ships are tremendously increasing. In order to maintain a smooth traffic, the waterways (rivers, canals, lakes) and harbors must be continually dredged. Dredging activities extract big quantities of sediments at very liquid state that are, under such states, improper for any uses. So, most of the time, before their re-use, dredged mud must be placed in a temporary disposal for drying and consolidation purpose. During that time, the dredged mud is consolidated under its self-weight, the water is drained out from the mud, the water content decreases, and the volume is significantly reduced. At the end of this process, the mud is more compact, less compressible and more easily transportable. Due to the increasing production of dredged material and to the limited space available, the management of disposal sites has become a major issue.[1] A prediction of the kinetics of consolidation and an optimization of the disposal equipment is therefore required.

When dredged mud is discharged on disposal sites, according to the solid concentration of the mixture, it may undergo one or a succession of three types of settling.[2] (i) "*The free sedimentation*" occurs when the solid concentration is very low, and the particles fall into the water independently of one another. The solid concentration in this case must be lower than 5–10 g/l.[3] This behavior can be modeled by means of the Stokes' law. (ii) "*The hindered sedimentation*" concerns the sedimentation with higher solid concentration such that particles start interacting between each other. Also, in cohesive sediments, flocs can even be created. This behavior can be explained by the Kynch's theory. (iii) "*Consolidation*" takes place when the solid concentration is getting even higher in order to encounter inter-particles contacts and starts behaving as a soil. The mud density corresponding to the transition between sedimentation and consolidation is called the "*structural density*". At this stage, the concept of effective stress can be used, but the consolidation theory developed

* Corresponding author.
E-mail address: bertrand.francois@ulb.ac.be (B. François).

https://doi.org/10.1016/j.gete.2021.100274
2352-3808/

by Terzaghi fails to represent the proper behavior due to the small strain assumptions. The Gibson's theory generalizes the Terzaghi's approach for nonlinear finite strain consolidation.[4,5]

In situations of sedimentation/consolidation occurring in disposal sites, the initial density of the discharged mud is close to the structural density, such that the initial condition is characterized by an effective stress close to zero. Consequently, the question of considering the three aforementioned types of settling must be raised. In a benchmark exercise aiming at modeling dredged mud settling in disposal sites,[6] the assumptions taken by most of the participants (excepted one) is to consider only the third phase (i.e. consolidation), through a Gibson-type model.

The Gibson theory was initially developed for pure fine-grained muds (i.e. cohesive materials) for which the consolidation is induced by the progressive dissipation of pore water pressure, inducing a mud densification due to the increase of effective stress. Also, pure muds have the advantage of having a relatively monodisperse grain size distribution, that does not create possible size segregation. In the situation of mixed sediments (mixing cohesive and non-cohesive materials, as usually the case for dredged mud), the validity of Gibson theory may be questioned. Some models considering mud–sand mixtures were proposed (e.g. Refs. 7–10), but due to the complexity of the involved processes, the matching with experimental observation could still be significantly improved, especially for large sand content. The two main effects of the presence of sand in the sedimentation/consolidation settling is that it modified the hindered sedimentation of cohesive materials and it may induce size segregation.[11] However, when starting from relatively dense concentration of sediments (higher than the structural density), those two effects are relatively limited.

During this self-weight consolidation process, the behavior is governed by two important material laws: the water permeability as a function of the void ratio, $k(e)$ and the compressibility, i.e. the void ratio as a function of the vertical effective stress, $e(\sigma'_v)$. Both expressions are highly non-linear and must be calibrated based on non-conventional laboratory tests. Due to the high deformation of the mud, its high initial void ratio and the light load applied to simulate self-weight consolidation, the conventional oedometer cannot be used to evaluate the mud compressibility. Through some adapted oedometer devices, large strain consolidation tests were developed.[12–14] As for conventional oedometer, the mud sample is contained in a cell, allowing only vertical deformation of the mud. The loading piston is not directly supported by the soil but is self-supported. Therefore, relatively low stress could be applied on the soil (around 0.01 kPa). Furthermore, a constant head or falling head apparatus is added to determine the permeability of the sample. The experiment consists of applying incremental loads, recording the vertical deformations and after each loading step, performing a permeability measurement. It has the advantage to be easy to perform but has the drawback of being time consuming. Another disadvantage is the possible sample disturbance due to the permeability test. Indeed, at high void ratio, the flux of water from the permeability determination can cause seepage forces and consolidation.

Alternatively, Hamilton and Crawford[15] introduced the concept of constant rate of deformation in the determination of the consolidation properties. The soil is loaded by a piston moving at constant speed, leading to a constant rate of strain in the sample. This loading technique has been implemented on devices measuring the large strain consolidation parameters.[16,17] It has the advantage to reduce the duration of the test and to be closer to the reality, i.e. continuous loading instead of discontinuous loading. Finally, Imai[18] proposed a consolidation technique based on seepage force. A constant head difference is applied across a mud sample which induces seepage force in the sample. These forces are converted into effective stress, which enable to consolidate the specimen. Nowadays, the desired water flow is provided by high accuracy pumps.

In order to reproduce in laboratory full-scale experiment of self-weight consolidation of dredged mud, with the purpose to measure the kinetics of consolidation, to calibrate materials parameters or to validate numerical models, some column experiments were developed (see for instance Refs. 19–21). It consists, most of the time, of a cylindrical plexiglass column where the mud is poured and allows undergoing consolidation in the column. Some measuring devices can be added to better characterize the ongoing behavior. In particular, pore water pressure and mud density can be measured during the consolidation process. Due to the transparency of the column, the position of the interface mud/water can be followed.

Pore water pressure can be measured, during the consolidation, by implementing some high accuracy pressure sensors on the wall of the column[22] or alternatively piezometric pipes.[23] For mud density measurement, X-ray or gamma ray technique can be used.[24] Alternatively, electrical resistivity can also be measured and correlated with the mud density.[25] Pedroni[26] summarizes most of the column experiments realized in the literature.

In most of the consolidation model, it is generally assumed that the drainage occurs through a perfectly permeable boundary condition. In practice, it is not necessarily the case for several reasons. First of all, the permeability of the drainage layer is usually limited and may be lower than the permeability of the mud at the start of the consolidation. Consequently, at early stage of consolidation, the permeability of the drainage layer could eventually play a significant role in the kinetics of consolidation. Secondly, the pore space of the drainage layer could be eventually clogged by the fine particles of the mud, which could still reduce its permeability.

Consequently, one of the objectives of this study is to evaluate the role of the drainage sand layer at the base of the consolidating dredged mud on the kinetics of consolidation of the mud. Because we start with a relatively high initial density of the mud (close to the structural density), as it is the case for most of disposal sites, we exclusively focus on consolidation process (and not the sedimentation). To do so, the problem is addressed in a twofold approach. On the one hand, a numerical model of large strain self-weight one-dimensional consolidation is developed and implemented through a finite difference method. The boundary condition at the base is adapted as a semi-permeable condition in order to reproduce the finite permeability of the draining layer. On the other hand, appropriate experimental tests, specifically developed for high void ratio and low effective stress conditions, are developed in order to calibrate the hydro-mechanical constitutive relations of the dredged mud. Then, a 2 meters high consolidation experiment is performed with the same mud but using three different sands at the base of the mud as draining layer. During this experiment, the excess pore water pressure profile, induced by the consolidation, is measured through high precision pressure transducers installed at different height of the consolidation column. For all those experiments, we used a mud, encompassing fine and coarse materials (47% > 74 μm), that is well representative of real sediments extracted from Belgian channels and rivers. Finally, the numerical predictions of the consolidation experiments are compared with experimental results and a sensitivity analysis is performed in order to evaluate the effect of the most important hydro-mechanical parameters on the kinetics of consolidation.

The main contribution of this work lies in the development of a unified and combined approach including both experimental characterization through specific devices adapted for low density materials (but still higher than the structural density) and numerical modeling. Also, one of the experiments, namely the kinematic permeameter, is totally innovative and provides accurate results for low density materials.

2. Numerical model

2.1. Governing equation

In this work, the non-linear large strain consolidation process is modeled based on the Gibson's theory.[4,5,27,28] Conventionally, this model is based on the concept of effective stress, in which the consolidation process is induced by a progressive mobilization of the effective stress related to a dissipation of pore water pressure. This is valid only when the void ratio is lower than the structural void ratio. Also, this Gibson theory is originally developed for fined-grained muds because the presence of coarse particles may enhance the process of size segregation that induces a vertical inhomogeneity in the consolidation column. In the present study, as it is usually the case in disposal sites, the initial water content is low enough such that the dredged mud is directly submitted to consolidation, while sedimentation does not occur. This is consistent with the observations of Bartholomeeusen et al.[6] using dredged soil from the Scheldt River (Antwerpen, Belgium) similar to the soil used in this research, i.e. similar grain size distribution, plasticity index and initial void ratio (≈ 4.5). Also, we have checked that the size segregation during the consolidation process is insignificant, as it will be discussed in Section 4.1.

The governing equations and the initial and boundary conditions are presented below while their discretization is reported in Appendix A.

The Gibson's non-linear large strain consolidation equation is as follow:

$$\left(\frac{\gamma_s}{\gamma_w}-1\right)\frac{d}{de}\left(\frac{k(e)}{1+e}\right)\frac{\partial e}{\partial z}+\frac{\partial}{\partial z}\left(\frac{k(e)}{\gamma_w(1+e)}\frac{d\sigma'_v}{de}\frac{\partial e}{\partial z}\right)+\frac{\partial e}{\partial t}=0 \quad (1)$$

where γ_w and γ_s are the unit weight of water and solid phase, respectively. z is the vertical coordinate (positive upward) and t is the time. σ'_v is the vertical effective stress. k is the coefficient of permeability. This equation is a second order non-linear partial differential equation with the void ratio $e(z,t)$ as unknown. The first and second terms have the form of advection and diffusion equations, respectively.

Because of the large strains undergone by the mud, a moving coordinate system, called reduced material coordinate system, is implemented. In order to relate at any time the reduced coordinate system (used in the governing equation) with the real-life system, three coordinates system (a, ξ, z) are defined, according to Fig. 1.

The following equations allow to relate the coordinate systems to each other[27–29]:

$$\frac{dz}{da}=\frac{1}{1+e_0} \quad (2)$$

$$\frac{d\xi}{dz}=1+e \quad (3)$$

2.2. Initial and boundary conditions

Solving Eq. (1) requires to define initial and boundary conditions. An initial constant void ratio is considered as an acceptable approximation for deposited dredged mud[29]:

$$e(z,t)=e_0 \quad \text{for } 0\le z\le H \text{ and } t=0 \quad (4)$$

where H is the total thickness of the consolidating layer at time $t=0$ in the material coordinate system. The top boundary condition will be set equal to the initial void ratio for all the time since this boundary is not loaded by any upper material or by any load:

$$e(H,t)=e_0 \quad \text{for } t>0 \quad (5)$$

Two cases were considered for the bottom boundary condition: the impermeable condition and the semi-permeable condition. The former does not allow any water flow through the base whereas the latter does but in a restrained manner depending on the permeability and the thickness of the draining layer. The impermeable boundary condition was only used to verify the model because only impermeable benchmark problems have been found in the literature. The semi-permeable boundary condition was developed to simulate the experiments carried out in the consolidation column with a bottom sand draining layer.

The impermeable boundary condition means that the velocities of the fluid and solid are nil. It corresponds to a zero hydraulic gradient. In the reduced material coordinate system, it yields

$$\frac{\partial u_w}{\partial z}+\gamma_w(1+e)=0 \quad (6)$$

where u_w is the hydrostatic pressure. Using the effective stress principle to transform water pressure into total stress and effective stress, combined with equilibrium equation stating that the total stress gradient is due to the density of the mud ($\gamma = e\gamma_w+\gamma_s$, in the reduced material coordinate system), Eq. (6) can be expressed as

$$\frac{\partial e}{\partial z}+(\gamma_s-\gamma_w)\frac{de}{d\sigma'_v}=0 \quad (7)$$

For the semi-permeable condition, the total pore pressure is the sum of the hydrostatic pore pressure and the excess pore pressure, such that in the material coordinate system, the space derivative yields:

$$\frac{\partial u_w}{\partial z}+\gamma_w(1+e)-\frac{\partial u}{\partial z}=0 \quad (8)$$

From the effective stress principle, the equilibrium equation, and multiplying each term by $\left(de/d\sigma'_v\right)$, this condition (8) is equivalent to

$$\frac{\partial e}{\partial z}=\left(\gamma_w-\gamma_s-\frac{\partial u}{\partial z}\right)\frac{de}{d\sigma'_v} \quad (9)$$

$\frac{\partial u}{\partial z}$ at the base of the mud can be obtained by stating that the amount of water leaving the mud is equal to the amount of water entering the sand layer. In the reduced material coordinate system:

$$\left[\frac{e}{1+e}(v_f-v_s)\right]_{mud}=\left[\frac{e}{1+e}(v_f-v_s)\right]_{sand} \quad (10)$$

where v_f and v_s are respectively the velocity of the fluid and the velocity of the solid grains.

With Darcy's law in the reduced material coordinate system, it is equivalent to

$$\left[\frac{k}{1+e}\frac{\partial u}{\partial z}\right]_{mud}=\left[\frac{k}{1+e}\frac{\partial u}{\partial z}\right]_{sand} \quad (11)$$

where u is the excess pore water pressure. This Eq. (11) allows to relate the excess pore water pressure gradient in mud to the excess pore water pressure gradient in sand, that is known if it is assumed that the base of the sand is fully drained.

2.3. Constitutive equations

Gibson's equation (1) requires the knowledge of the constitutive laws, i.e. the permeability–void ratio and the effective stress–void ratio relationships. So far, it has been stated that the constitutive laws must be unique function of the void ratio, i.e. $k=k(e)$ and $\sigma_v'=\sigma_v'(e)$. Several mathematical expressions have been developed by authors to fit as close as possible the experimental results. Logarithm function, exponential function,

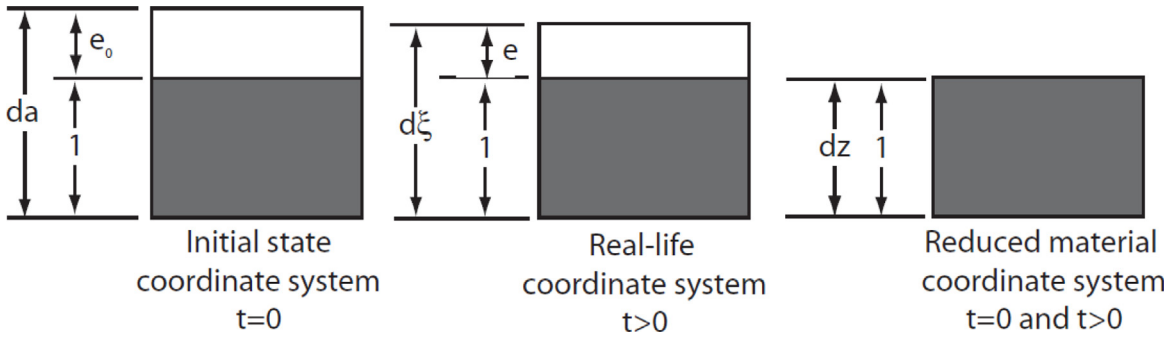

Fig. 1. Different coordinate systems.
Source: adapted from[27].

power function, extended power function and Weibull function are the relationships the most often encountered in the literature. Ahmed et al.[30] have presented a summary of the different existing mathematical forms of the constitutive laws and their respective scope. Those constitutive relations will be calibrated on independent experimental tests in Section 4.1.

3. Experimental set-ups

This section presents the non-conventional experimental set-ups that were developed for the determination of material parameters governing the relations between permeability and void ratio, as well as void ratio and effective stress. Because of high void ratios, high permeabilities and low effective stress levels, conventional oedometers or permeameters are not suitable for the present study. Two specific devices have been developed: a hydraulic column and a kinematic permeameter. In addition, the consolidation column that was developed and used to perform the large strain consolidation experiments is also presented in this section.

Both hydraulic column and kinematic permeameter allow to obtain the two essential constitutive relations involved in the Gibson equation: the permeability and the vertical effective stress as functions of the void ratio ($k = k(e)$ and $\sigma_v' = \sigma_v'(e)$). However, hydraulic column is more dedicated for high density materials (i.e. low void ratio) while kinematic permeameter is for low density material (i.e. high void ratio, just below the structural void ratio). Consequently, those two tests are complementary.

3.1. Hydraulic column

This system is inspired by the concept of seepage-induced consolidation developed by Sridharan et al.[31]. The main idea is to impose a constant head difference at the two ends of a soil sample. This difference induces a hydraulic gradient through the soil which forces the water to flow. The seepage will generate effective stresses in the soil skeleton which will result in a consolidation. Instead of inducing consolidation with "physical" load (weights) like in a conventional oedometer, here the loading is induced by the hydraulic gradient. When the flow is steady, the deformation can be obtained by measuring the height of the sample while the permeability can be determined directly from the flow seeping out of the soil sample.

Fig. 2a shows the experimental apparatus. Two columns of 64 mm of inner diameter and lengths of 11 cm and 145 cm, respectively, are used. The shortest column accommodates the mud while the longest is used to impose the desired height of water. It was chosen to use two pieces of columns, connected hermetically together, in order to reduce the height when the mud sample is poured to the bottom. The base accommodates a porous stone, a cavity and an outlet to drain the water towards the draining line. A peristaltic pump supplies some water into the column whereas an overflow maintains a constant water level in the column. 130 g of dry mud is mixed homogeneously with 140% of water and is poured into the lower part of the column and is allowed to consolidate due to self-weight. Finally, the column is carefully filled with water.

The theoretical explanation of this seepage-induced consolidation, developed by Imai[18] and Terzaghi et al.,[32] is as follow. When z is positive downward, the hydraulic head is expressed according to Bernoulli equation as

$$h = -z + \frac{u_w}{\gamma_w} \tag{12}$$

So, the gradient of pore water pressure with depth is

$$\frac{du_w}{dz} = \left(\frac{dh}{dz} + 1\right)\gamma_w \tag{13}$$

Consequently, the effective stress gradient can be obtained from the total stress and pore water pressure gradient

$$\frac{d\sigma_v'}{dz} = \frac{d\sigma_v}{dz} - \frac{du_w}{dz} = \gamma - \left(\frac{dh}{dz} + 1\right)\gamma_w = \gamma' - \frac{dh}{dz}\gamma_w \tag{14}$$

where γ' is the submerged density of the soil ($\gamma' = \gamma - \gamma_w$). In the experiment, the hydraulic gradient dh/dz being negative (in order to produce a downward seepage), Eq. (14) shows that the effective stress profile is increased due to the downward seepage. Fig. 2b shows schematically the experimental set-up with the hydraulic head and effective stress profiles.

If we assume that at the start of the experiment, the mud has already experienced its self-weight consolidation, only the second term of Eq. (14) must be considered in the experiment. Because of the linear evolution of induced effective stress from zero to a maximum value at the base of the specimen, the equivalent induced effective stress is half of the effective stress at the base. Consequently, the link between equivalent effective stress and applied difference of hydraulic head is

$$\sigma_{v,eq}' = \frac{\gamma_w \Delta H}{2} \tag{15}$$

Equivalent effective stress from 0.125 kPa to 4 kPa are applied in 6 steps, by doubling the magnitude at every step, which corresponds to a difference of hydraulic head from 0.025 m to 0.815 m. Additionally, permeability can be deduced during the test by measuring the quantity of water collected at the outlet of the drainage circuit, through the classical constant head permeameter formula.

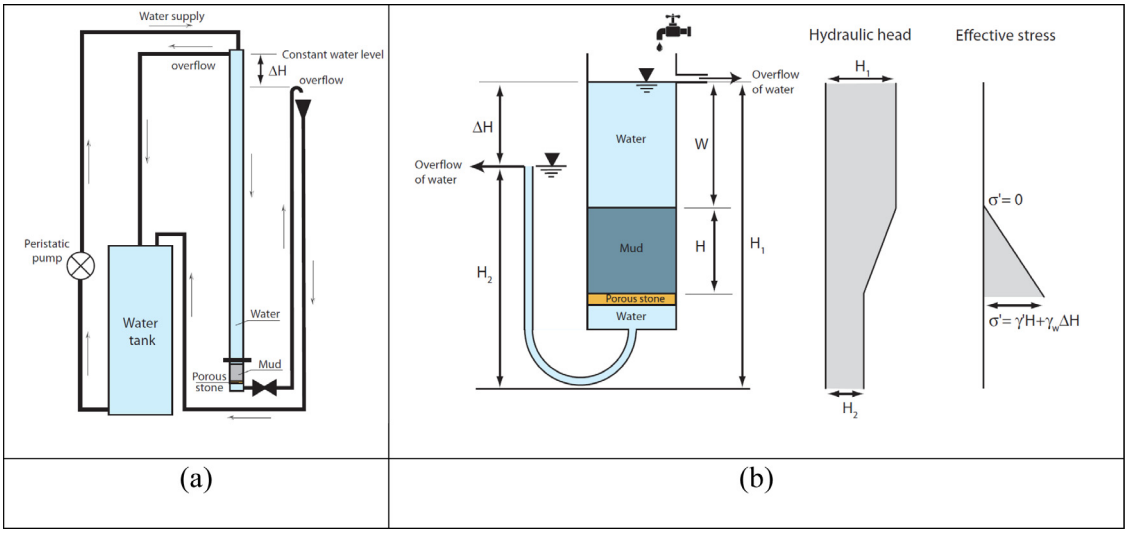

Fig. 2. (a) Schematic view of the hydraulic column set-up; (b) Schematic explanation of the increase of effective stress gradient induced by the downward seepage.

3.2. Kinematic permeameter

The hydraulic column is an efficient technique but, as explained in Section 3.1, it can only be implemented on a mud sample already consolidated under self-weight leading to a lack of information during this self-weight consolidation. To overcome this problem, the kinematic permeameter was developed. In this experiment, the permeability and compressibility of a mud sample is determined based on the intrinsic properties of the consolidating specimen, i.e. the velocity of the interface mud/water and the measured excess pore water pressure. This is an original contribution because, to the authors' knowledge, this system has never been developed anywhere else. It is especially well-adapted for the determination of the permeability and the effective stress at high void ratio, just below the structural void ratio.

The experimental apparatus (Fig. 3a) is composed of two main parts: a cylindrical vessel and a graduated burette, connected by a flexible pipe which can be closed by a manual valve. The vessel has a height of 150 mm and an inner diameter of 53 mm.

The protocol starts by pouring water into the vessel and the water is allowed to flow into the burette. Equilibrium of water between vessel and burette is checked. The valve is then closed, and the water is emptied from the vessel. The theoretical excess pore water pressure at the base of the future sample is calculated and its equivalent height of water is determined. This quantity of water is manually added to the burette in order to be at balanced pressure when the vessel will be filled with mud. The mud sample is then prepared with a water content of 140% and a dry mass of 130g. It is poured into the vessel. Its height and level are rapidly recorded. Directly after, the valve is opened to equalize the pressure. These operations have to be realized quickly to begin the measurements at the start of the consolidation. The level of the interface and the water level in the burette are recorded at regular time interval.

Initially, at the start of the consolidation, the effective stress is nil, and the pore water pressure equals the total stress. Then, as consolidation occurs, the pore water pressure progressively decreases, the volume occupied by the mud decreases and the water is drained through the top to create a supernatant water layer. This drainage takes place because of the hydraulic gradient induced by the excess pore water pressure. Fig. 3b represents the occurring phenomenon from initial time t_0 to a given time t_1.

Darcy's law can be applied

$$\frac{\Delta V_w}{A\Delta t} = k\frac{dh}{L} = k_{mean}\frac{u_{mean}}{L_{mean}\gamma_w} \tag{16}$$

where ΔV_w is the increment of water volume drained out of the specimen during the elapsed time Δt. This volume corresponds to volume of the supernatant water layer. A is the section of the specimen, dh is the variation of hydraulic head between top and bottom of the specimen (see Fig. 3b), L_{mean} is the mean thickness of the specimen during the time increment, u_{mean} is the mean excess pore water pressure measured at the base of the specimen during the time increment. Reversing Equation (16), the mean permeability of the mud at any time can be deduced:

$$k_{mean} = \frac{\Delta V_w L_{mean}\gamma_w}{u_{mean}A\Delta t} \tag{17}$$

The corresponding effective stress is deduced from the total stress and the pore water pressure as follow:

$$\sigma'_{v,mean} = \gamma' L_{mean} - u_{mean} \tag{18}$$

This effective stress at the base must be divided by two to have an equivalent constant effective stress instead of a triangular profile

$$\sigma'_{v,mean,eq} = \frac{\sigma'_{v,mean}}{2} \tag{19}$$

The mean void ratio can be simply obtained through the mean thickness of the specimen over the time increment. In such a way, the permeability and the effective stress can be related to the void ratio.

3.3. Consolidation column

The primary purpose of a consolidation column is to track the evolution of the settlement of a material during the consolidation process. To do so, the column is a cylindrical tube made of translucent Plexiglas to follow visually the mud/water interface. However, additionally, the evolution of the excess pore water pressure profile during the consolidation process is a valuable information. Therefore, in addition to the interface position measurement, pressure sensors (PX26-005GV, 0–34 kPa and an accuracy of 0.25% full scale; from Omega) connected to a pressure measurement system (Gage Panel Meter DP25B-S from

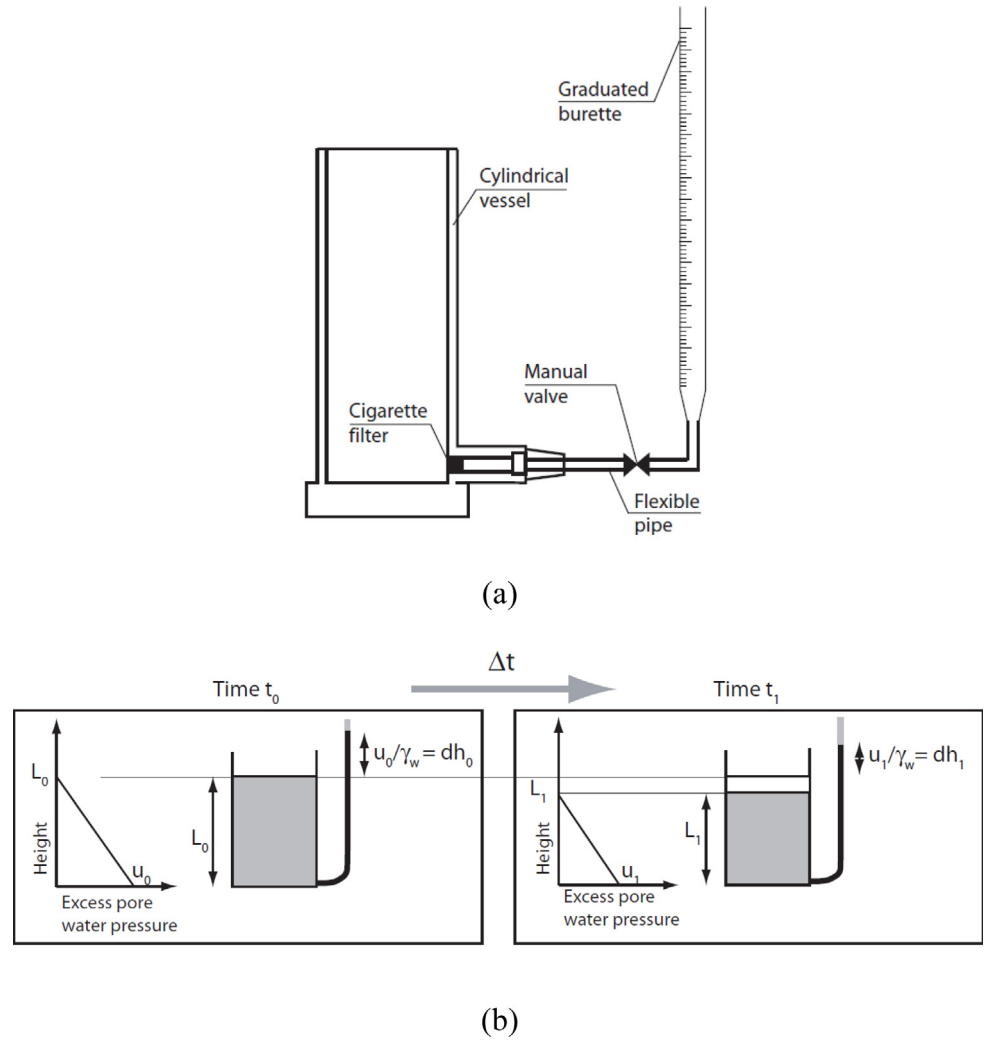

Fig. 3. (a) Sketch of the kinematic permeameter; (b) Schematic explanation of the dissipation of excess pore water pressure and subsequent increases of effective stress in the kinematic permeameter experiment.

Omega) were implemented on the column. The full experimental apparatus is represented on Fig. 4a.

The column, made of Plexiglass, has an inner diameter of 200 mm and a total height of 2.1 m. The base includes a porous stone and a cavity underneath it to drain the water out. The porous stone is 1 cm-thick and is conventionally assumed to oppose negligible resistance to the drainage flow. Pressure transducer were connected to the inner face of the column by an assembly of connection pieces, as detailed in Fig. 4b.

The consolidation experiments were performed at constant hydrostatic pore pressure such that the possible water flows are only induced by the excess pore water pressure due to the consolidation process. To do so, the level of water in the consolidation column is maintained constant. It is made possible by connecting a vertical pipe filled with water to the base of the column. The column and the pipe were similar to a siphon. A valve at the base of the pipe allows to keep the water in the vertical pipe during the pouring of the mud.

The sand layer is installed at the base of the column on a thickness of 27 cm. This layer is topped by gravel to protect the sand layer against the erosion during the pouring of the mud. Initially, to saturate the sand, the column is filled with water while the tap of the draining line stays open to enable the water in the draining line to reach the same level as the one in the column.

After one day under water, to start the experiment, the tap of the draining line is closed to keep the water in and the column is emptied of water until the upmost level of the gravel layer. Then, the mud at a water content of 140% (see the mud preparation protocol in Section 4.1) is transferred from the tank to the column by means of buckets. The mud is poured from the top of the column. Once the column is full of mud, the tap of the draining layer is immediately opened to equalize the hydrostatic pressures. At the desired time, pore water pressures and interface position are measured.

4. Material properties

4.1. Dredged mud

This study has been initially motivated by the need to evaluate the ability of several sands to act as a drainage layer at the base of Belgian dredged mud disposal site. Consequently, we have selected a dredged mud that is well representative of real sediment extracted from Belgian channels and rivers. The slurry has been obtained from dredging activities in the Belgian navigable rivers and canals. First of all, the slurry is sieved at 5 mm to remove "trash elements" (piece of wood, plastic, big gravel or stone …). The sieved slurry is then dried. Once completely dried, the mud is weighted and mixed with the required amount of water in a

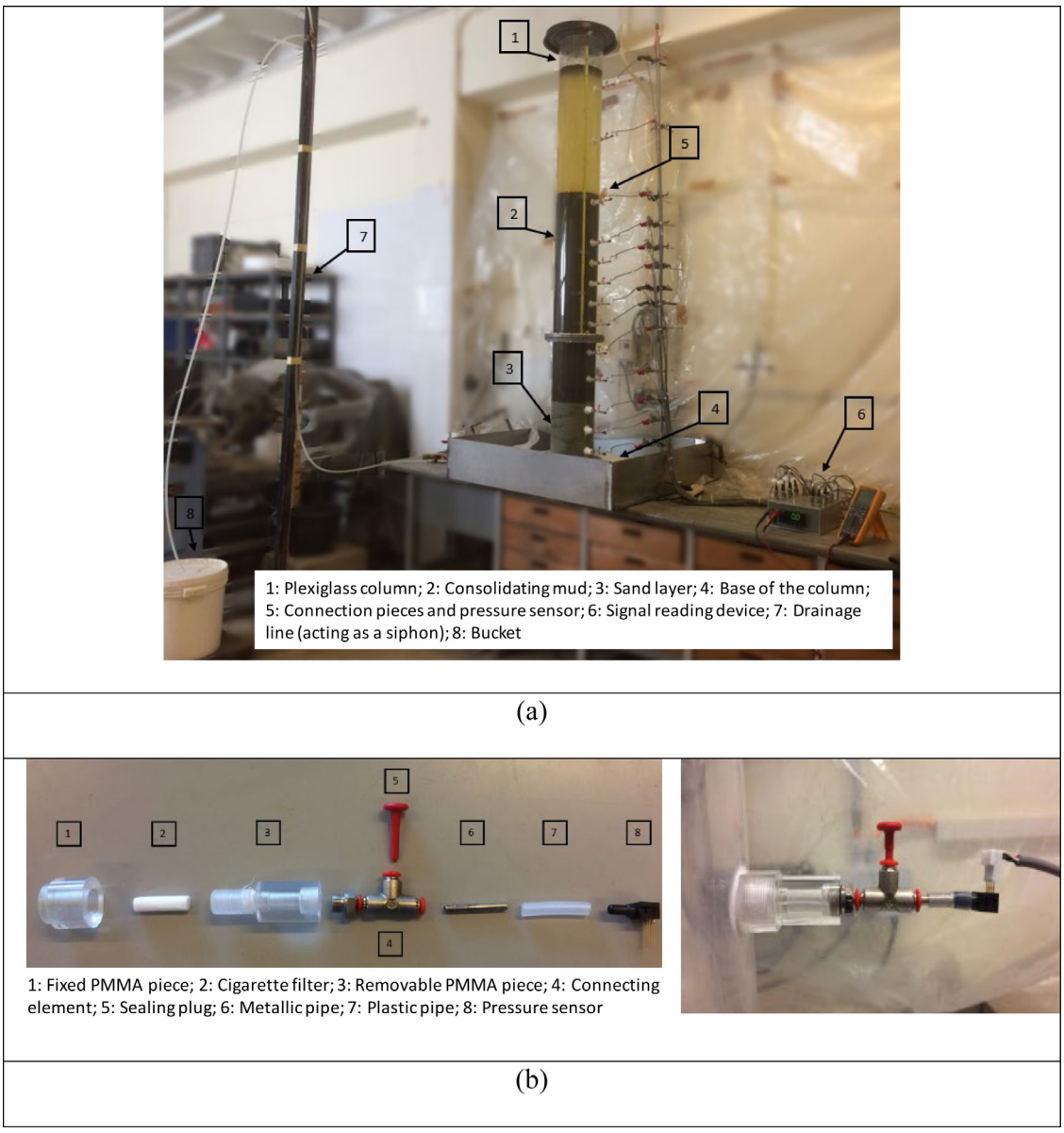

Fig. 4. (a) View of the consolidation column; (b) Details of the connections of the pressure sensors with the wall of the column.

large tank to reach the desired water content of 140%. With a unit weight of solid particles of 27.1 kN/m^3, the initial void ratio, e_0, is 4.58. The mud stays in the tank, in contact with water, for three days, being regularly stirred with a hand mixer for plaster, to ensure a perfect saturation and the homogeneity of the water distribution. For the consolidation column experiment, the mud is transferred from the tank to the column by means of 5-liter buckets while the mud in the tank is continuously mixed with the hand mixer. The mud in the buckets is poured from the top of the column.

The grain size distribution of the mud is reported in Fig. 5. Because we aim at using a representative slurry, as dredged in Belgian rivers and channels, the selected mud encompasses both fine and coarse particles. The presence of clay particles is relatively limited (6% $<$ 2 μm) while the size of the grain is mostly concentrated in the range of silt particles (47% between 2 μm and 60 μm) and sand particles (37% between 60 μm and 2 mm).

Due to the well-graded character of the grain size distribution curve, we were expecting possible size segregation during the

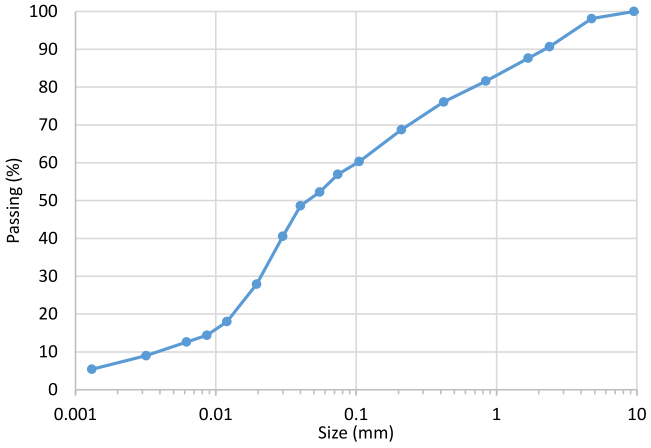

Fig. 5. Grain size distribution of the mud.

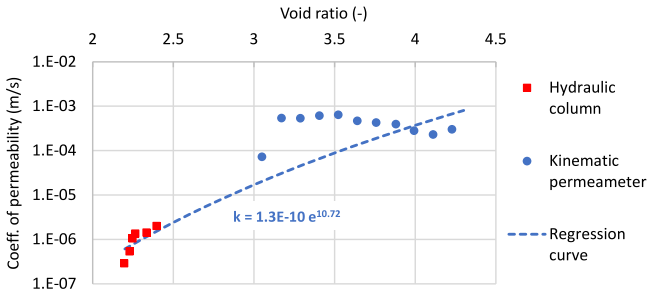

Fig. 6. Measured water permeability of the mud as a function of the void ratio, measured by the kinematic permeameter and the hydraulic column, and the proposed regression curve using a power law.

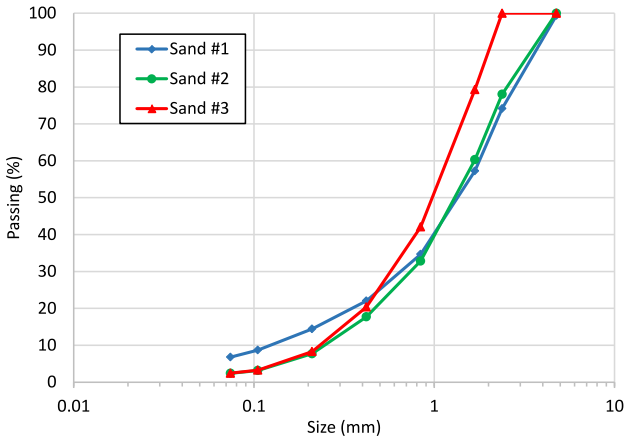

Fig. 8. Grain size distribution of the three sands, used as drainage layer.

sedimentation/consolidation experiments. Consequently, at the end of each consolidation column experiment, we extracted small mud fragment, 3 cm above the bottom and 3 cm below the top of the mud column at the end of the consolidation process. The fine content (%<74 μm) was equal to 45% at the bottom, 53% at the top, for an average of 52% in the full column. This result demonstrates a slight, but not significant, difference in fine contents which means that the size segregation can be neglected. This is probably because the initial void ratio of the mud was close to the structural void ratio, such that sedimentation is negligible with respect to consolidation. Consequently, we may assume that the particle size of the mud remains homogeneous during the experiments, such that the properties of the mud deduced from kinematic permeameter and hydraulic column can be extrapolated to the consolidation column experiment.

4.1.1. Permeability vs void ratio

The kinematic permeameter and the hydraulic column allow to determine the water permeability of the mud at high and moderate void ratio, respectively. Fig. 6 shows the obtained results. The water permeability obtained from the kinematic permeameter, for void ratio from 4.2 to 3 (i.e. at high void ratio) does not follow a clear trend with the void ratio but the order of magnitude ($\approx 10^{-4}$ m/s) is consistent with results from literature. In particular Bartholomeeusen et al.[33] measured water permeability of 10^{-4} m/s to 10^{-5} m/s for void ratios from 4 to 3 on a dredged mud with similar grain size distribution. At moderate void ratio (from 2.4 to 2.1), the hydraulic column provides a consistent trend of water permeability as a function of void ratio.

The experimentally-observed evolution of the permeability with void ratio exhibits drastic variation in a small range of void ratio. Typically, the permeability changes of several orders of magnitude when void ratio goes from 2.5 to 2.2. As a consequence, the best fit mathematical expression should encounter steep gradient that would induce stability and convergence problems of the numerical resolution scheme. Consequently, the constitutive law $k(e)$ has been calibrated through a power law as the best regression curve, from the least square method, through the experimental points:

$$k = 1.310^{-10} e^{10.72} \tag{20}$$

Fig. 6 shows that the regression curve does not fit closely with the results of kinematic permeameter and that several relations could fit the experimental results. Consequently, a sensitivity analysis on the effect of this $k(e)$ relation on the consolidation behavior of the mud will be considered in Section 5.3.

4.1.2. Effective stress vs void ratio

Similarly, the kinematic permeameter and the hydraulic column allow also to determine the compressibility of the mud at high and moderate void ratio, respectively. The evolution of the void ratio with respect to the effective stress is plotted in Fig. 7. The obtained trend is consistent with the expected results. The mud is highly compressible at high void ratio for which the void ratio drastically decreases for a low increase of effective stress. Then, for moderate void ratio, the compressibility is progressively reduced. In literature, a power law is generally used as the constitutive relation between void ratio and effective stress. However, in this study, a hyperbolic model has been preferred starting from

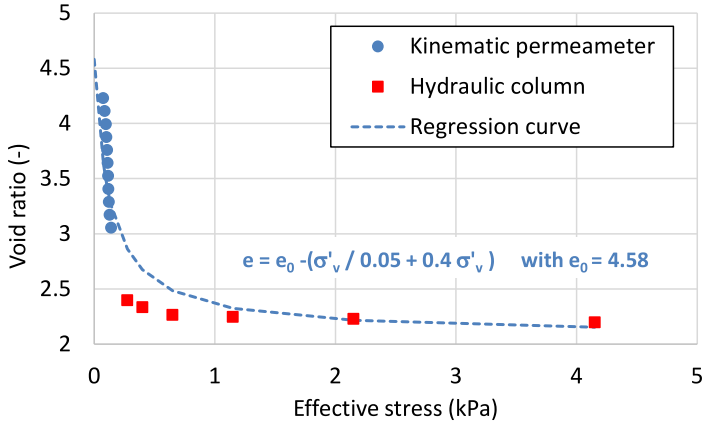

Fig. 7. Measured void ratio of the mud as a function of the vertical effective stress, measured by the kinematic permeameter and the hydraulic column.

Table 1
Water permeability of the three sands used as drainage layer during the consolidation experiments.

	Water permeability (m/s)
Sand #1	4.1 E−6
Sand #2	1.5 E−5
Sand #3	9.3 E−6

the value of initial void ratio at zero effective stress ($e_0 = 4.58$).

$$e = e_0 - \frac{\sigma'_v}{0.05 + 0.4\sigma'_v} \tag{21}$$

This expression uses two parameters that have a physical meaning: one of them controls the slope of the evolution of $e(\sigma'_v)$ at low effective stress (i.e. at high void ratio) while the other defines the void ratio at high effective stress. To study the effect of this $e(\sigma'_v)$ law on the kinetics of consolidation of the mud, a sensitivity analysis is performed in Section 5.3.

4.2. Drainage layer — sand

As explained in the introduction, the permeability of the drainage layer at the base of the mud is usually high but still limited. So, one of the objectives of this study was to evaluate experimentally if the type of sand that acts as a draining layer at the base of the mud plays a significant role in the kinetics of drainage. Consequently, three types of sand were used with a good contrast of permeability. Their grain size distribution is shown in Fig. 8 while their water permeability, measured from conventional falling head permeameters, is reported in Table 1. The water permeabilities are consistent with the grain size distribution of the three sands. Sand #1 has a lower permeability due to the presence of 5% of fine particles (<74 μm) while sand #2 has a lower permeability than sand #3 because sand #2 is sieved at 2 mm.

5. Self-weight consolidation behavior

5.1. Experimental results

The self-weight consolidation tests have been performed with the three different sands as drainage layer at the base. Each test lasted at least 6 days and the excess pore water pressures were measured regularly, at different depths in the consolidating mud. Also, the evolution of the water/mud interface was tracked as a function of time. Results are reported in Fig. 9.

The sand layer acts as a semi-permeable boundary. Consequently, at initial time, the excess pore water pressure in the mud is linear (zero at the top and maximum at the bottom boundary) and is equals to γ'z, where γ' is the submerged unit weight of the mud and z is the depth from the mud surface. When consolidation starts, the sand acts rapidly as a draining layer and the excess pore water pressure is dissipated from both top and bottom sides. Most of the dissipation of excess pore water pressure takes place during the first day, while during the next days, the process tends asymptotically to zero excess pore water pressure. Concerning the water–mud interface level, most of the settlement takes place during the first day while during the next days, the settlement is almost negligible.

The effect of the sand permeability used as draining layer on the global consolidation behavior is not really pronounced. The comparison of Fig. 9 a, b and c reveals that the slight variations of the curve are not consistent with the sand permeability. The variability of the excess pore water pressure profile between the different tests are more ascribed to the variability of the mud and of the setting up of the mud in the column from one test to another. This will be confirmed through the numerical modeling is Section 5.2.

5.2. Model prediction

The model presented in Section 2, with the material parameters deduced in Section 4, permits to simulate the self-weight consolidation experiment with the three different sands as drainage layer. The obtained numerical predictions are compared with experimental results in terms of excess pore water pressure profiles and settlement of the water–mud interface, in Fig. 10, for the three different sands used as draining bottom layer.

First, it is observed that the magnitude of sand permeability at the base of the mud does not affect significantly the kinetics of consolidation of the mud predicted by the model. The three sands produce almost identical evolutions of the settlement of the mud/water interface while the excess pore water pressure profiles are very similar but still with a small variation of profile at low heights (closed to the sand layers). The sand with the lowest permeability (Sand #1) produces a slightly slower dissipation of excess pore water pressure during the first hours.

According to the model prediction, it is concluded that the range of variation of the sand permeability does not allow to produce any significant effect on the global consolidation process, even if very slight effects are observed in the bottom of the column at short term.

Secondly, the evolution of the mud settlement is satisfactorily predicted, excepted at very short term where the numerical simulations predict a much faster settlement than the experiment. This could be due to the calibration of the constitutive law (permeability and compressibility as a function of void ratio) at high void ratio. Nevertheless, the numerical prediction reaches the correct final settlement, meaning that the constitutive relation between effective stress and void ratio is well calibrated for low void ratio.

Finally, the predicted excess pore water pressure profiles match relatively well with the experimental measurements. The numerical predictions after 0.02 and 0.17 days are able to reproduce the magnitude and the location of the peak of excess pore water pressure. However, at longer term, after 0.88 days, the numerical predictions underestimate the remaining excess pore water pressure in the mud. This is probably due to the overestimation of the permeability of the mud at low void ratio (in Fig. 6, the fitted curve is higher than the experimental points for the two lowest considered void ratios).

5.3. Sensitivity analysis

Due to the relative uncertainties on the constitutive relations and also the unperfect regression curves fitting the experimental results, it is proposed to perform a sensitive analysis on the effect of the relations $k(e)$ and $\sigma'(e)$ on the kinetics of consolidation of the mud. This sensitivity analysis is performed considering sand #1 as the drainage layer. Anyway, as seen before, the characteristics of the sand do not affect significantly the kinetics of consolidation, at least in the tested range of the permeability of the sand.

For the relation between permeability and void ratio, the power law (Eq. (22)) is used with 3 sets of parameters as illustrated in Fig. 11. The sets of parameters are reported in Table 2.

$$k = Ae^B \tag{22}$$

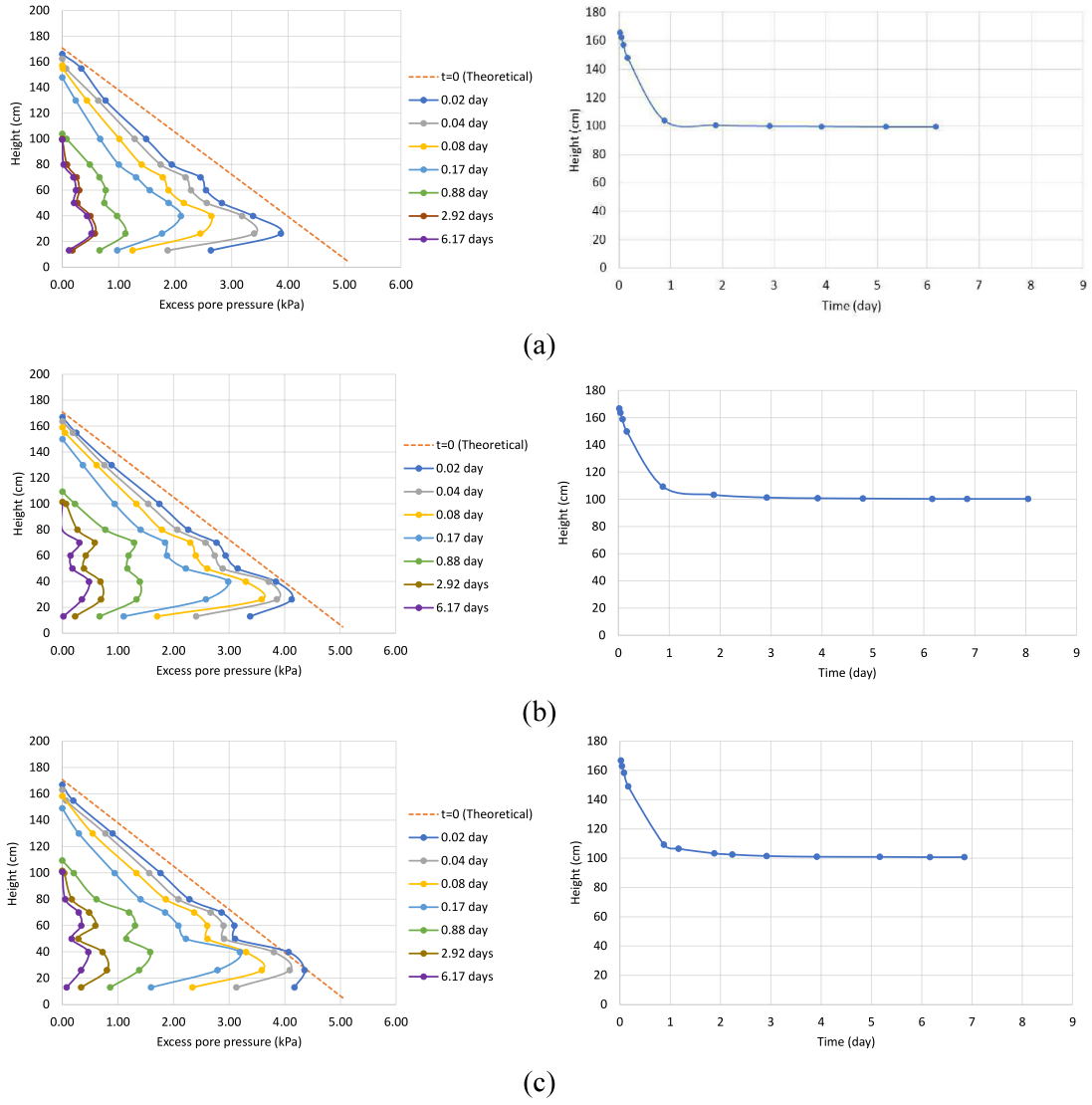

Fig. 9. Obtained results of the consolidation column experiments with the three different sands used as drainage layer. (a) Sand #1; (b) Sand #2; (c) Sand #3. Left column: Excess pore water pressure profile; Right column: Evolution of the height of mud/water interface measured from the base of the mud (i.e. the top of the drainage layer).

Table 2
Set of parameters of Eq. (22) used for the sensitivity analysis.

	A (m/s)	B (–)
Case 0	1.3E−10	10.72
Case 1	1.12E−11	13.74
Case 2	4.34E−10	9.26

For low void ratio, the value of the permeability is maintained unchanged because the obtained experimental measurements can be considered as realistic while the sensitivity analysis is essentially performed on the effect of the permeability at high void ratio in order to cover the range of measured experimental values.

The obtained numerical predictions of the time evolution of the settlement, compared with experimental results are reported in Fig. 12. It is observed, as expected, that the reduction of the permeability of the mud at high void ratio makes the consolidation slower during the first day (i.e. Case 2 is slower than cases 0 and 1). But still, the experimental results remain slower than the numerical prediction with the lowest permeability. However, the final state, at the end of the consolidation process, is not affected by the permeability of the mud (i.e. the three settlement curves converge to the same final settlement).

In terms of mud compressibility as a function of the void ratio, sensitivity analysis on the coefficient of the hyperbolic function is performed:

$$e = e_0 - \frac{\sigma'_v}{C + D\sigma'_v} \tag{23}$$

Coefficient C controls the magnitude of void ratio at high effective stress, while coefficient D affects the slope of the constitutive curve σ'(e) at low effective stress (i.e. at high void ratio). Fig. 13 illustrates the different used relations with the set of parameters reported in Table 3, while Fig. 14 shows the obtained time evolution of the settlement and excess pore water pressure profile for the different sets of parameters. The numerical predictions show that the compressibility of the mud (i.e. relation between effective stress and void ratio) affects both transient and final states. During the consolidation process, a lower void ratio for the same effective stress induces a lower permeability which, in turn, reduces the speed of consolidation. Consequently, case a is

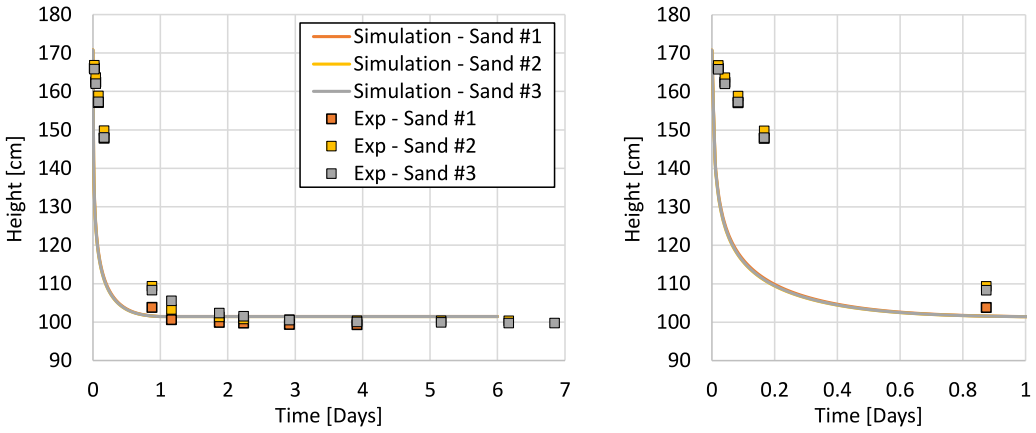

(a)

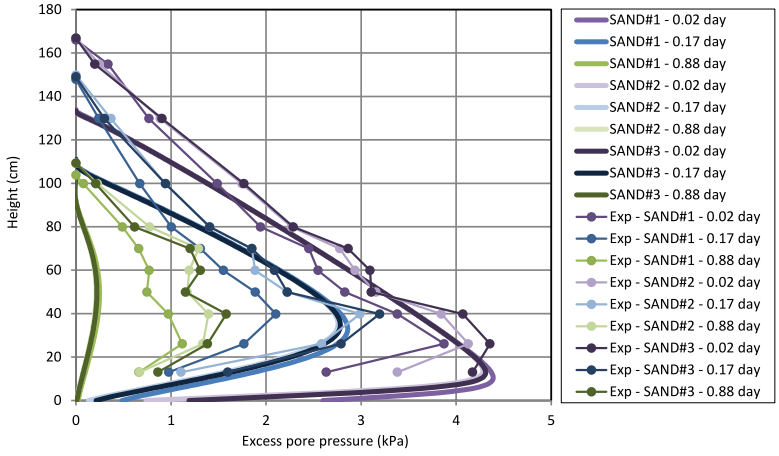

(b)

Fig. 10. Comparison of the model predictions with the experimental results, for the three different sands used as draining bottom layer. (a) Evolution of the height of mud/water interface measured from the base of the mud (the model prediction curves are superimposed); (b) Excess pore water pressure profile (the slight difference in model predictions for the three sands are visible at the low heights close to the base).

slower that case 0, itself slower than case b. At final state, the relation that considers a lower void ratio for the same effective stress induces a lower final height of the mud–water interface.

This sensitivity analysis shows that none of the selected set of parameters is able to significantly improve the prediction of the rate of settling at short term. Case 2 that considers a globally lower permeability of the mud allows to reduce slightly the rate of settling but the predictions are still much faster than the experimental observations. We may note that the predictions of the pore water pressure profile after 0.17 days are relatively good, especially for cases 1 and b (Fig. 12b and Fig. 14b) which means that the evolution of effective stress profile at short term is also well predicted. However, despite the correct pore water pressure profile prediction at 0.17 days, the model overestimates, with a factor of more than 2, the settling of the mud–water interface. Consequently, this overestimation of the rate of settling at short term must be attributed to the compressibility relation, $\sigma'(e)$, at short term. As already presumed by Bartholomeeusen et al.[6], based on experimental observations of Leroeuil et al.[34] dedicated to small-strain consolidation, at such a short term the effective stress–void ratio relationship is prone to time-dependent effects. So, if the compressibility of the mud is strain-rate dependent, the

Table 3
Set of parameters of Eq. (23) used for the sensitivity analysis.

	C (–)	D (kPa)
Case 0	0.05	0.4
Case a	0.05	0.38
Case b	0.1	0.4

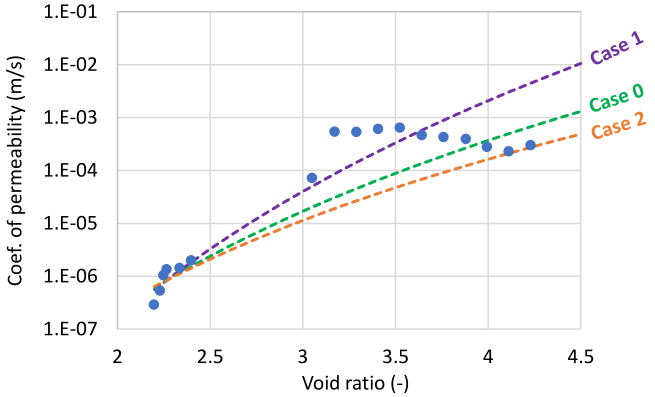

Fig. 11. Sensitivity analysis on the relation between the coefficient of permeability and the void ratio. The used parameters are summarized in Table 2.

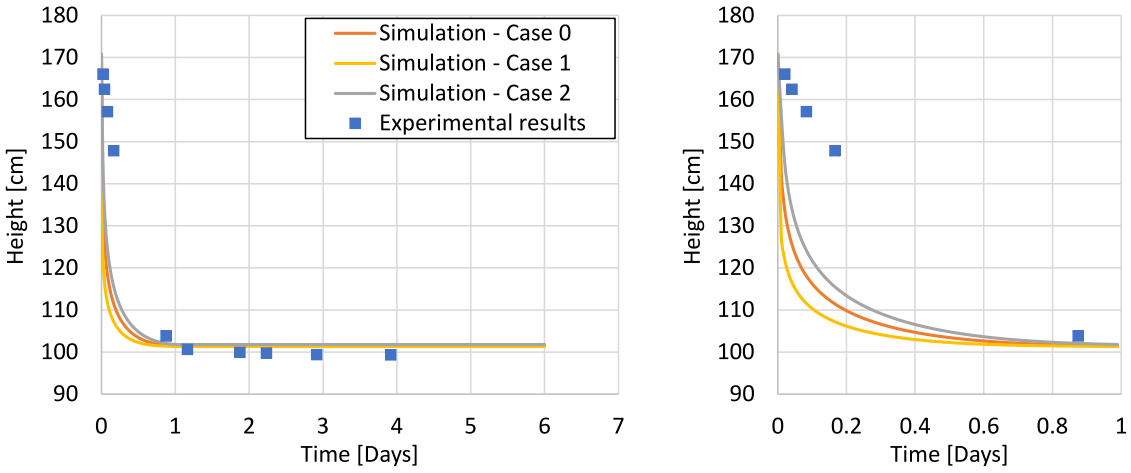

(a)

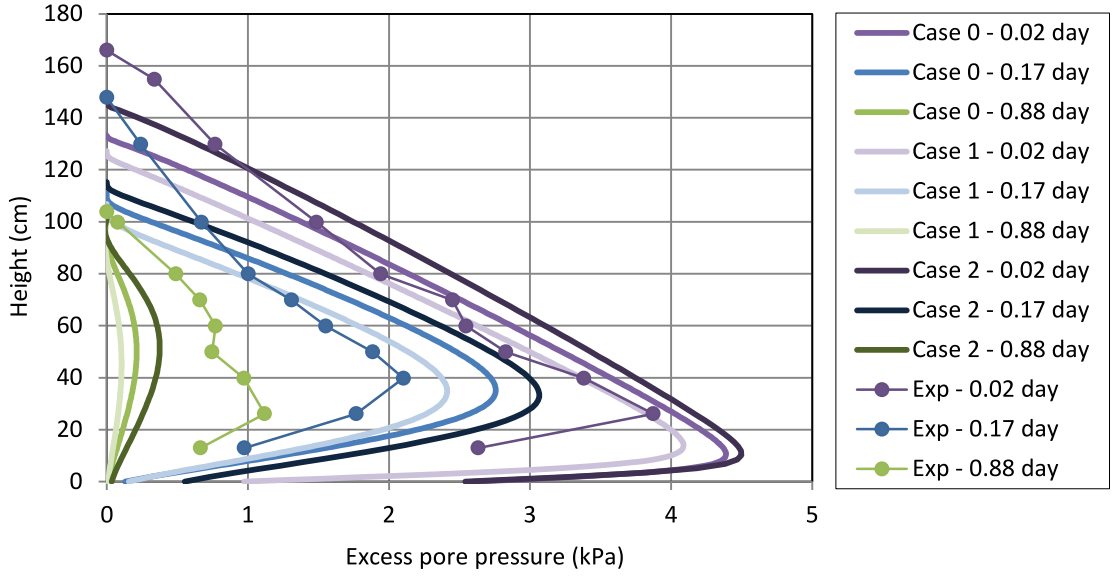

(b)

Fig. 12. Effect of the relation between permeability and void ratio on (a) the settlement of the water–mud interface and (b) the excess pore water pressure profile for sand #1 as drainage layer. Cases 0, 1 and 2 correspond to different fitting curves of the permeability–void ratio relationship (as plotted in Fig. 11)

large strain experienced in a short period of time in the consolidation column induces a huge strain rate that is not tackled by the experiments developed for the material characterization. At the end, the constitutive relationship deduced at moderate strain-rate overestimates the compressibility of the mud experienced in the consolidation column at large strain rate.

6. Conclusions

For dredging activities, the lack of space to store the dredged mud and the continuously increasing amount of dredged waste have led to an optimization of the disposal sites. It is therefore essential to better understand, to characterize and to predict the consolidation behavior of the dredged mud. This consolidation process involves highly non-linear relation between the permeability of the mud and its void ratio, as well as variable compressibility, also depending on void ratio.

This study has combined an experimental investigation, involving three original experimental set-ups, and a numerical study of the large strain consolidation of a dredged mud as a function of the drainage condition at the base.

Two experimental tests, namely the hydraulic column and the kinematic permeameter, aimed at calibrating the constitutive relations governing the consolidation of the mud while the last experiment, i.e. the consolidation column, was designed to study the kinematics of the one-dimensional large strain consolidation of the mud for different draining sands at the base. The rate of settlement and the evolution of excess pore water pressure profiles in the mud is monitored during the consolidation.

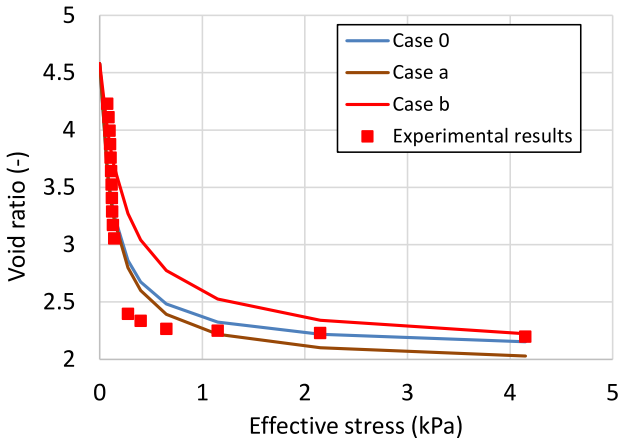

Fig. 13. Sensitivity analysis on the relation between the void ratio and the vertical effective stress. The used parameters are summarized in Table 3.

Then, the Gibson's equation, describing the large strain consolidation process, has been solved through a finite difference method in order to model the consolidation column experiment, based on materials parameters deduced from the other independent tests. A semi-permeable boundary condition at the bottom of the mud was considered in order to evaluate the effect of the permeability of the sand, at the base. Finally, a sensitivity analysis on the permeability and compressibility of the mud has been carried out.

The model prediction, with parameters determined from independent experiments, matches relatively well with the experimental observation during the consolidation column experiment, especially in term of excess pore water pressure profile. The rate of settlement is overestimated by the model at short term (during the first day of consolidation) while the final settlement is very well predicted. Also, it is concluded that the permeability of the sand at the base plays an insignificant role on the kinetics of consolidation as long as this permeability remains higher that the permeability of the consolidated mud. From a practical point of view, this means that, for modeling purpose, when the permeability of the drainage layer at the base is lower than the permeability of the consolidated mud, the boundary condition at the base may be assumed as fully drained without significant overestimation of the kinetics of consolidation.

Despite convincing results in terms of experimental characterization and numerical prediction, this study revealed some important issues that must be careful considered to properly tackle the complex hydro-mechanical processes occurring during large strain consolidation of dredged mud. (i) The applicability of the Gibson's theory for large-strain consolidation requires that the mud remains homogeneous all along the pouring and consolidation process. This is only possible if we remain below the structural void ratio, such that the contact between particles avoid size segregation to occur. (ii) The highly non-linear constitutive relations appear to be a challenge for numerical resolution. In particular, the strong gradient in $k(e)$ and σ'(e) relationships requires a very fine time discretization combined with smoothed fitting curves to avoid instability of the numerical scheme. (iii) The mud characterization in term of permeability *vs* void ratio and effective stress *vs* void ratio requires some specific experimental set-ups to work with very low effective stress range and high void ratio. Moreover, it is expected that the compressibility law can be significantly affected by strain-rate effect, especially at early stage of consolidation (when the rate of settling is high). This implies that complex experimental set-ups must be developed to characterize this phenomenon and that the Gibson theory must be adapted to consider a time-dependent effect in the σ'(e) relationship. This is a perspective of this study.

CRediT authorship contribution statement

Bertrand François: Conceptualization, Methodology, Validation, Supervision, Resources, Project administration, Funding acquisition, Writing – original, Writing – review & editing, Visualization. **Gilles Corda:** Formal analysis, Investigation, Data curation, Writing – original, Writing – review & editing.

Declaration of competing interest

The authors declare that they have no known competing financial interests or personal relationships that could have appeared to influence the work reported in this paper.

Acknowledgments

The authors express their deep appreciation to Fabiano Pucci and Nicolas Canu, for their technical support in the development of experimental set-ups and their help for the carrying out of the experiments.

Appendix A. Numerical implementation of the gibson model

A.1. Governing equations

To solve the Gibson's Equation (1), the explicit finite difference scheme proposed by Wang et al.[21] and Cao et al.[35] is adopted here. The unknown is the void ratio at any time and any depth, i.e. $e(z,t)$. The solution at a later time is calculated based on the current time. The Gibson equation can be re-written as

$$\frac{\partial e}{\partial t} = \frac{\partial}{\partial z}\left(g\,(e)\,\frac{\partial e}{\partial z}\right) - B\,(e)\,\frac{\partial e}{\partial z} \tag{A.1}$$

where

$$g\,(e) = \frac{-k}{\gamma_w\,(1+e)}\,\frac{d\sigma'_v}{de} \tag{A.2}$$

$$B\,(e) = \left(1 - \frac{\gamma_s}{\gamma_w}\right)\frac{d}{de}\left(\frac{k}{1+e}\right) \tag{A.3}$$

The reduced material coordinate z is positive downward. Note the change of sign in the last term of Eq. (A.1) with respect to Gibson Equation (1) for which z was positive upward.

The incremental indices for time and space are j and i such $z_i = i\Delta z$ with $i = 0, 1, \ldots, Nz$ and $t_j = j\Delta t$ with $i = 0, 1, \ldots, Nt$. The points in the space and time domain are equally spaced. The left-hand side of Eq. (A.1) is approximate by a forward Euler scheme. A central difference is used for the first term on the right-hand side (that is a diffusion term) while an upwind scheme is used for the second term on the right-hand side (that is advective term). At the end, the full discretized equation is

$$e_i^{j+1} = e_i^j + \left[\frac{1}{\Delta z^2}\left(g_{i+1/2}^j\left(e_{i+1}^j - e_i^j\right) - g_{i-1/2}^j\left(e_i^j - e_{i-1}^j\right)\right) - \frac{B_i^j + \left|B_i^j\right|}{2}\,\frac{e_{i+1}^j - e_i^j}{\Delta z} - \frac{B_i^j - \left|B_i^j\right|}{2}\,\frac{e_i^j - e_{i-1}^j}{\Delta z}\right] dt \tag{A.4}$$

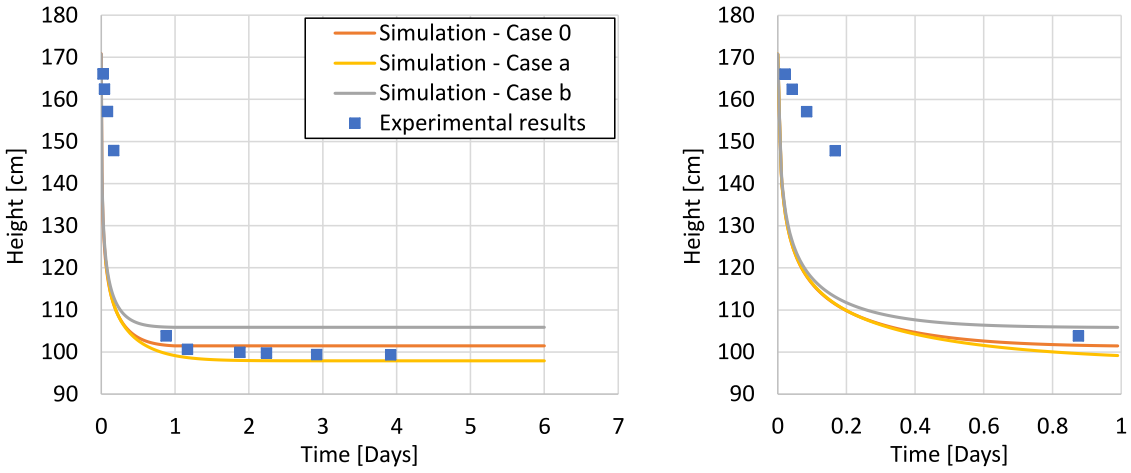

(a)

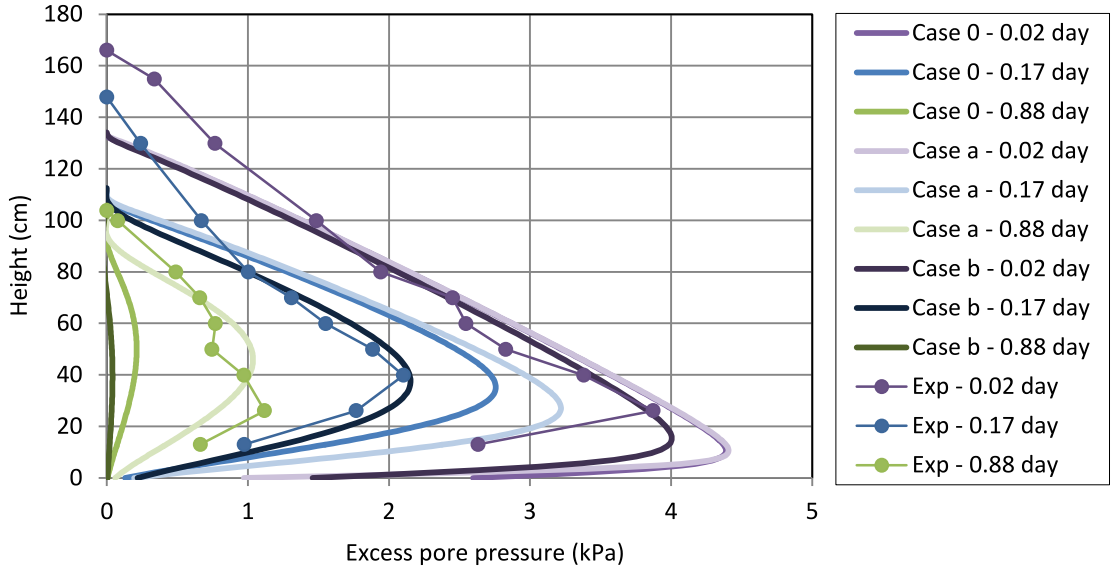

(b)

Fig. 14. Effect of the relation between void ratio and effective stress on (a) the settlement of the water–mud interface and (b) the excess pore water pressure profile for sand #1 as drainage layer. Cases 0, a and b correspond to different fitting curves of the void ratio-effective stress relationship (as plotted in Fig. 13).

A.2. Initial and boundary conditions

The boundary condition at the base requires an additional fictive node (N_{z+1}) to express the void ratio at the base (e_{Nz}) as a function of the node N_{z+1}.

For the impermeable base, Eq. (7) is discretized as:

$$e_{i+1}^{j} = e_i^j + \Delta z\,(\gamma_s - \gamma_w)\left(\frac{de}{d\sigma_v'}\right)_i^j \tag{A.5}$$

For the semi-permeable base condition, Eq. (9) becomes

$$e_{i+1}^{j} = e_i^j + \Delta z\left(\gamma_s - \gamma_w + \left(\frac{\partial u}{\partial z}\right)_i^{j-1}\right)\left(\frac{de}{d\sigma_v'}\right)_i^j \tag{A.6}$$

Note the change of sign in Eqs. (A.5) and (A.6) with respect to Eqs. (7) and (9) due to the positive z coordinate in the downward direction.

For the semi-permeable condition, it is required to express the gradient of excess pore water pressure in the sand (represented by the node N_{z+1}). This can be done by considering that the excess pore water pressure at the base of the sand is nil. Consequently,

$$\left(\frac{\partial u}{\partial z}\right)_{Nz+1} = \frac{u_{Nz}}{x/(1+e_{sand})} \tag{A.7}$$

where x is the length of drainage, i.e. the thickness of the sand layer.

A.3. Stability, convergence and consistency

Consistency requires, when Δt and/or Δz tend to zero, that the truncation errors tend to zero and therefore the numerical solution should approach the true solution of the partial differential equation.[35,36] The finite difference approximation is said stable if an error, occurring during the computation, is not increased

as the process proceeds. Convergence implies that the numerical solution tends to the true solution. These three requirements are formulated with the help of two criteria limiting the size of the mesh. Indeed, if Δt and Δz are small enough the numerical solution is stable, consistent and converges.

Cargill[27,28] presented these two criteria for the large strain consolidation equation solved with explicit finite difference:

$$\Delta z \leq \frac{2g\,(e)}{-B\,(e) + \frac{\partial g(e)}{\partial z}} \tag{A.8}$$

and

$$\Delta t \leq \frac{\Delta z^2}{g\,(e)} \tag{A.9}$$

After the use of the numerical implementation, it appeared that the two criteria (A.8) and (A.9) were necessary but not sufficient to the convergence of the procedure. Actually, the Gibson's equation is advective dominance such that

$$g\,(e) \ll |B\,(e)| \tag{A.10}$$

Consequently, the upwind scheme should satisfy the Courant–Friedrich–Lewy condition:

$$\frac{|B\,(e)|\,\Delta t}{\Delta z} \leq 1 \tag{A.11}$$

This criterion means that the size of the time step Δt should be smaller than the time needed for the wave to travel the size of the space step Δz. At the end, the three conditions (A.8)–(A.10) must be fulfilled to guarantee the stability, consistency and convergence of the numerical scheme.

References

1. Van Mieghem J, Smits J, Sas M. Large-scale dewatering of fine-grained dredged material. *Terra Et Aqua*. 1997:21–28.
2. Imai G. Settling behavior of clay suspension. *Soils Found*. 1980;20(2):61–77.
3. Mehta AJ, Hayter EJ, Parker WR, Krone RB, Teeter AM. Cohesive sediment transport. I: Process description. *J Hydraul Eng*. 1989;115(8):1076–1093.
4. Gibson RE, England GL, Hussey MJL. The theory of one-dimensional consolidation of saturated clays: 1. Finite non-linear consolidation of thin homogeneous layers. *Géotechnique*. 1967;17(3):261–273.
5. Gibson RE, Schiffman RL, Cargill KW. The theory of one-dimensional consolidation of saturated clays. II. Finite nonlinear consolidation of thick homogeneous layers. *Can Geotech J*. 1981;18(2):280–293.
6. Bartholomeeusen G, Sills GC, Znidarcic D, Van Kesteren W, Merckelbach LM, Pyke R, Carrier III WD, Lin H, Penumadu D, Winterwerp H, Masala S, Chan D. Sidere: numerical prediction of large-strain consolidation. *Géotechnique*. 2002;52(9):639–648.
7. Toorman EA. Sedimentation and self-weight consolidation: general unifying theory. *Géoetchnique*. 1996;46(1):103–113.
8. Merckelbach L, Kranenburg C. Equations for effective stress and permeability of soft mud-sand mixtures. *Géotechnique*. 2004;54(4):235–243.
9. Van LA, Pham Van Bang D. Hindered settling of sand/mud flocs mixtures: from model formulation to numerical validation. *Adv Water Resour*. 2013;53:1–11.
10. Le Hir P, Cayocca F, Waeles B. Dynamics of sand and mud mixtures: a multiprocess-based modelling strategy. *Cont Shelf Res*. 2011;31:S135–S149.
11. Grasso F, Le Hir P, Bassoullet P. Numerical modelling of mixed-sediment consolidation. *Ocean Dyn*. 2015;65(4):607–616.
12. Sheeran DE, Krizek RJ. Preparation of homogeneous soil samples by slurry consolidation. *J Mater*. 1971;6(2):356–373.
13. Monte JL, Krizek RJ. One-dimensional mathematical model for large-strain consolidation. *Géotechnique*. 1976;26(3):495–510.
14. Jeeravipoolvarn S, Masala S, Zhang C, Moore T. Revisiting the large strain consolidation test for oil sands. In: *Proceedings Tailings and Mine Waste*. 2015.
15. Hamilton J, Crawford C. Improved determination of preconsolidation pressure of a sensitive clay. In: *Papers on Soils 1959 Meetings*. 1960: 254–71.
16. Umehara Y, Zen K. Constant rate of strain consolidation for very soft clayey soils. *Soils Found*. 1980;20(2):79–95.
17. Lee K. Consolidation with constant rate of deformation. *Géotechnique*. 1981;31(2):215–229.
18. Imai G. Development of a new consolidation test procedure using seepage force. *Soils Found*. 1979;19(3):45–60.
19. Torfs H, Mitchener H, Huysentruyt H, Toorman E. Settling and consolidation of mud/sand mixtures. *Coast Eng*. 1996;29(1–2):27–45.
20. Guo SJ, Zhang FH, Song XG, Wang BT. Deposited sediment settlement and consolidation mechanisms. *Water Sci Eng*. 2015;8(4):335–344.
21. Wang L, Sun J, Zhang M, Yang L, Li L, Yan J. Properties and numerical simulation for selfweight consolidation of the dredged material. *Eur J Environ Civil Eng*. 2018:1–16.
22. Sills GC. Development of structure in sedimenting soils. *Phil Trans R Soc A*. 1998;356(1747):2515–2534.
23. Berlamont J, Van den Bosch L, Toorman EA. Effective stresses and permeability in consolidating mud. In: *Coastal Engineering Proceedings*. 1992: 2962–75.
24. Been K, Sills GC. Self-weight consolidation of soft soils: an experimental and theoretical study. *Géotechnique*. 1981;31(4):519–535.
25. Cuthbertson A.J.S O, McCarter WJ, Starrs G. Monitoring and characterisation of sandmud sedimentation processes. *Ocean Dyn*. 2016;66(6–7):867–891.
26. Pedroni L. *étude Expérimentale Et Numérique de la Sédimentation Et de la Consolidation Des Boues de Traitement Des Eaux Acides* [Ph.D. thesis]. Canada: École Polytechnique de Montréal; 2011.
27. Cargill KW. *Consolidation of Soft Layers By Finite Strain Analysis*. Technical Report; Geotechnical Laboratory U.S. Army Engineer Waterways Experiment Station; 1982.
28. Cargill KW. Prediction of consolidation of very soft soil. *J Geotech Eng*. 1984;110(6):775–795.
29. Stark TD, Choi H, Schroeder PR. Settlement of dredged and contaminated material placement areas. I: Theory and use of primary consolidation, secondary compression, and desiccation of dredged fill. *J Waterw Port Coast Ocean Eng*. 2005;131(2):43–51.
30. Ahmed SI, Siddiqua S. A review on consolidation behavior of tailings. *Int J Geotech Eng*. 2014;8(1):102–111.
31. Sridharan A, Prakash K. Simplified seepage consolidation test for soft sediments. *Geotech Test J*. 1999;22(3):235–244.
32. Terzaghi K, Peck RB, Mesri G. *Soil Mechanics in Engineering Practice*. John Wiley & Sons; 1996.
33. Bartholomeeusen G. *Compound Shock Waves and Creep Behaviour in Sediment Beds* [Ph.D. thesis]. UK: Oxford University; 2003.
34. Leroueil S, Kabbaj M, Tavenas F, Bouchard R. Stress–strain–strain rate relation for the compressibility of sensitive natural clays. *Géotechnique*. 1985;35(2):159–180.
35. Cao Y, Yang J, Xu G, Xu J. Analysis of large-strain consolidation behavior of soil with high water content in consideration of self-weight. *Adv Civil Eng*. 2018.
36. Lynch DR. *Numerical Partial Differential Equations for Environmental Scientists and Engineers: A First Practical Course*. Springer; 2004.